

Determination of the Higgs properties with the ATLAS detector

Tamara Vazquez Schroeder, on behalf of the ATLAS Collaboration

McGill University

E-mail: tamara.vazquez.schroeder@cern.ch

Combined measurements of Higgs boson production cross sections and branching fractions are presented using the $H \rightarrow \gamma\gamma$ and $H \rightarrow ZZ^* \rightarrow 4\ell$ decay channels based on 36.1 fb^{-1} of proton-proton collision data recorded at $\sqrt{s} = 13 \text{ TeV}$ by the ATLAS experiment at the LHC. No significant deviations from the Standard Model expectations are observed.

*EPS-HEP 2017, European Physical Society conference on High Energy Physics
5-12 July 2017
Venice, Italy*

1. Motivation

The Higgs boson discovery in July 2012 by the ATLAS [1] and CMS [2] experiments was a major milestone in the Large Hadron Collider’s (LHC) physics program and a breakthrough in our knowledge of high-energy particle physics. Since then, a wide range of measurements of its properties have been performed using proton-proton collision data produced by the LHC at centre-of-mass energies of $\sqrt{s} = 7$ and 8 TeV in Run 1 [3], and at $\sqrt{s} = 13$ TeV in Run 2 using 13.3 fb^{-1} of data by the ATLAS experiment [4] and using 35.9 fb^{-1} of data by the CMS experiment [5], all of them consistent with the Standard Model (SM) predictions. The combination of Higgs-boson decay channels maximises the precision of these measurements, allows more model-independent measurements, and constrains the coupling to the Higgs boson with less assumptions.

The combined measurements of Higgs boson production cross sections and branching fractions presented here use the $H \rightarrow \gamma\gamma$ and $H \rightarrow ZZ^* \rightarrow 4\ell$ decay channels and an integrated luminosity of 36.1 fb^{-1} of proton-proton collision data recorded at $\sqrt{s} = 13$ TeV by the ATLAS experiment at the LHC during 2015 and 2016 [6]. The dataset consists of approximately three times the luminosity of the results in Ref. [4], allowing improved measurements of Higgs boson production and decay.

2. Input analyses

The input decay channels used in this combination are the “golden” Higgs discovery channels: $H \rightarrow \gamma\gamma$ [7] and $H \rightarrow ZZ^* \rightarrow 4\ell$ [8]. The analyses of the individual channels separate the measured events into exclusive kinematic and topological categories. Each of these categories targets a specific Higgs boson production mode: gluon fusion (ggF), $gg \rightarrow H$, weak vector-boson fusion (VBF), $qq' \rightarrow qq'H$, associated production with a W or Z boson, $q\bar{q}' \rightarrow VH$, and associated production with a pair of top quarks, $q\bar{q}/gg \rightarrow t\bar{t}H$.

The $H \rightarrow \gamma\gamma$ analysis defines 31 exclusive event categories. The categories are structured hierarchically to prioritise the selection of signal events from processes with the smallest production cross sections, $t\bar{t}H$ and tHX , followed by VH where categories are distinguished by the vector-boson decays, and finally VBF and ggF.

The $H \rightarrow ZZ^* \rightarrow 4\ell$ analysis defines 9 event categories to distinguish the $t\bar{t}H$, VH , VBF, and ggF production modes. The analysis reconstructs the intermediate Z bosons using their decays to electrons and muons, and requires the four-lepton invariant mass to be between 118 and 129 GeV.

3. Measurements and results

Combined cross section measurements are reported in various global fit models in order of increasing granularity of Higgs boson production modes and kinematics. First, the total inclusive production cross section ($pp \rightarrow H + X$) and the ratio of the total signal yield with respect to the SM prediction (μ) are presented in Sections 3.1 and 3.2. Then, the inclusive cross sections of individual production processes and their ratios are reported in Sections 3.3 and 3.4. Finally, cross sections in kinematic regions of the production processes in the framework of simplified template cross sections (STXS) are detailed in Section 3.5. To characterise deviations from the SM expectations,

the results are translated into measurements of the multiplicative coefficients κ_i of Higgs-boson couplings in the SM, as shown in Section 3.6.

3.1 Total cross section

The total cross section is measured based on the inclusive event yields in each decay channel. The event yields are corrected for detector effects, the fiducial acceptance relative to the full phase space, and branching fractions. The corrections are derived using the SM predictions for the cross section ratios between the different production modes. The total $pp \rightarrow H + X$ cross section at centre-of-mass energy of 13 TeV is $57_{-5.9}^{+6.0}(\text{stat.})_{-3.3}^{+4.0}(\text{syst.})$ pb, in good agreement with the SM prediction at N3LO QCD of $55.6_{-3.4}^{+2.4}$ pb [9]. The measurement is statistically limited.

3.2 Global signal strength

The global signal strength μ is determined from a fit to a single parameter defined as the ratio of the total observed yield to its SM expectation, $\mu = \frac{\sigma \times B}{(\sigma \times B)_{SM}}$. This parameter is applied as a single scaling factor to all production processes and decay modes. The global signal strength is measured to be $\mu = 1.09 \pm 0.12 = 1.09 \pm 0.09(\text{stat.})_{-0.05}^{+0.06}(\text{exp.})_{-0.05}^{+0.06}(\text{th.})$. The combined μ value lies within the signal strengths of the individual measurements in each decay mode: $\mu = 0.99 \pm 0.14$ in $H \rightarrow \gamma\gamma$ and $\mu = 1.28_{-0.19}^{+0.21}$ in $H \rightarrow ZZ^* \rightarrow 4\ell$. The event categorisation reduces the statistical uncertainty relative to the total cross section measurement. The measurement is consistent with the SM prediction with a p-value of $p_{SM} = 47\%$. The dominant theoretical uncertainties originate from the QCD scale and PDF variations, whereas the dominant experimental uncertainties are due to luminosity and electron/photon energy resolution.

3.3 Production cross sections

A simultaneous fit is performed for the cross sections of ggF, VBF, VH , and $t\bar{t}H$ for $|y_H| < 2.5$ and assuming SM branching fractions. The measurement of bbH is included in ggF, and the measurement of tH is included in $t\bar{t}H$. The process $gg \rightarrow ZH$ is fully attributed to ZH .

Figure 1 (left) shows the production cross section measurement results. The cross section for the VBF production is $7.9_{-1.8}^{+2.1}$ and has the largest deviation from its SM expectation, $3.52_{-0.07}^{+0.08}$ [9]. The four-dimensional compatibility between the measurement and the SM prediction corresponds to a p-value of $p_{SM} = 5\%$.

Figure 1 (right) shows the measured likelihood contours in the VBF and ggF cross section plane from the individual fits in $H \rightarrow \gamma\gamma$ and $H \rightarrow ZZ^* \rightarrow 4\ell$, as well as for the combined fit. The cross sections for VH and $t\bar{t}H$ are profiled with the data. The two-dimensional compatibility between the measurement and the SM prediction corresponds to a p-value of $p_{SM} = 3\%$.

3.4 Ratios of cross sections and branching fractions

A combined fit to data is performed with the production cross sections of VBF, VH , and $t\bar{t}H$ normalised to ggF, and with the branching ratio of $H \rightarrow \gamma\gamma$ normalised to $H \rightarrow ZZ^* \rightarrow 4\ell$. The product of the cross section and the branching fraction can be expressed in terms of these ratios:

$$\sigma_i \times BR_f = \sigma_{ggF} \times BR_{H \rightarrow 4\ell} \times \frac{\sigma_i}{\sigma_{ggF}} \times \frac{BR_f}{BR_{H \rightarrow 4\ell}} \quad (3.1)$$

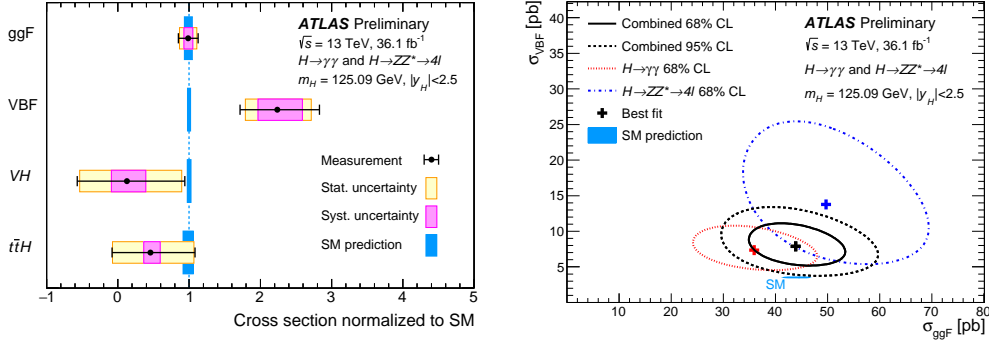


Figure 1: (Left) cross sections for ggF, VBF, VH, and $t\bar{t}H$ normalised to the SM predictions and measured with the assumption of SM branching fractions. The black error bars and pink and yellow boxes show the total, systematic, and statistical uncertainties in the measurements, respectively. The blue bands indicate the theoretical uncertainties in the predictions [6]. (Right) measured likelihood contours in the σ_{VBF} versus σ_{ggF} plane in $H \rightarrow \gamma\gamma$ (red) and $H \rightarrow ZZ^* \rightarrow 4\ell$ (blue), as well as their combination (black) [6], together with the SM prediction (light blue) [9].

where i is a Higgs-boson production process, f is a final state, and BR_f is the branching fraction for the Higgs boson to decay into f .

Table 1 shows the measurements of $\sigma_{ggF} \times BR_{H \rightarrow 4\ell}$, $\sigma_{VBF}/\sigma_{ggF}$, σ_{VH}/σ_{ggF} , $\sigma_{t\bar{t}H}/\sigma_{ggF}$, and $BR_{H \rightarrow \gamma\gamma}/BR_{H \rightarrow 4\ell}$. The five-dimensional compatibility between the measurements and the SM predictions corresponds to a p-value of $p_{SM} = 3\%$.

Quantity	Result	Uncertainty			SM prediction	
		Total	Stat.	Exp.		
$\sigma_{ggF} \cdot B_{4\ell}$ [fb]	6.6	$+1.2$ -1.0	$+1.1$ -1.0	± 0.4	± 0.2	$5.6^{+0.3}_{-0.4}$
$B_{\gamma\gamma}/B_{4\ell}$	12.5	$+2.8$ -2.3	$+2.6$ -2.2	$+0.9$ -0.7	± 0.2	18.1 ± 0.2
$\sigma_{VBF}/\sigma_{ggF}$ [10^{-2}]	21.5	$+8.5$ -6.3	$+7.3$ -5.6	$+2.8$ -1.7	$+3.6$ -2.2	$7.9^{+0.4}_{-0.6}$
σ_{VH}/σ_{ggF} [10^{-2}]	0.2	$+4.5$ -3.4	$+4.2$ -3.2	$+1.2$ -0.9	$+0.9$ -0.4	$4.5^{+0.2}_{-0.3}$
$\sigma_{t\bar{t}H}/\sigma_{ggF}$ [10^{-2}]	0.7	$+1.0$ -0.9	$+1.0$ -0.9	$+0.2$ -0.1	± 0.1	1.3 ± 0.1

Table 1: Best-fit values and uncertainties of $\sigma_{ggF} \times BR_{H \rightarrow 4\ell}$ and the ratios of cross sections and branching fractions.

3.5 Simplified template cross sections

The simplified template cross section (STXS) framework defines a set of kinematic regions for each production process and combines these with the ratios of branching fractions for the various decay channels in order to probe the properties of the Higgs boson. The splitting of the production modes is based on kinematic variables such as the jet multiplicity, the transverse momentum of the Higgs boson, and the transverse momentum of the leading jet. The basic STXS scheme has been agreed between the ATLAS experiment, the CMS experiment, and theorists within the LHCXSWG [9] and is schematised in Figure 2 (“stage-1”). The cross sections are then measured in these mutual exclusive regions of the phase space called “truth bins”. As a temporary solution to

increase the sensitivity to SM production and minimise correlations, some bins have been merged for the current results. All regions require $|y_H| < 2.5$. This framework allows to maximise experimental sensitivity while minimising theory dependence. Additionally, these cross sections can be interpreted in various beyond-the-SM models.

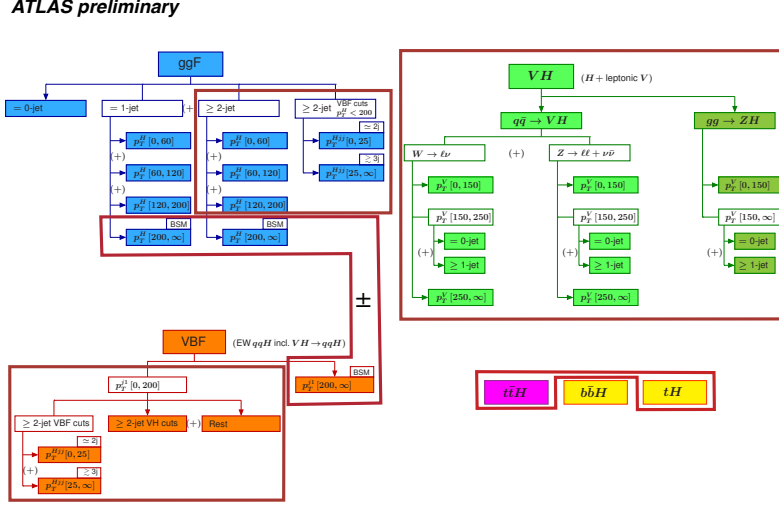


Figure 2: The merged STXS stage-1 regions defined for the measurements [9]. All regions surrounded by red boxes are merged, except for the sum and difference indicated by the “ \pm ” sign connecting two merged $gg \rightarrow H$ regions with one $qq \rightarrow Hqq$ region. The bbH region is merged with the $gg \rightarrow H$ bins [6].

Table 2 shows the fitted values of the ratio of branching ratios $B_{H \rightarrow \gamma\gamma}/B_{H \rightarrow 4\ell}$ and of the simplified template cross sections. The results show good overall agreement with the SM predictions. The ten-dimensional compatibility between the measurement and the SM prediction corresponds to a p-value of $p_{SM} = 9\%$.

Measurement region	Result	Uncertainty			SM prediction
		Total	Stat.	Syst.	
$B_{\gamma\gamma}/B_{4\ell}$	12.5	$^{+2.8}_{-2.3}$	$\begin{pmatrix} +2.6 \\ -2.2 \end{pmatrix}$	$\begin{pmatrix} +0.8 \\ -0.6 \end{pmatrix}$	18.1 ± 0.2
$gg \rightarrow H$ (0-jet)	29.7	$^{+7.3}_{-6.4}$	$\begin{pmatrix} +6.6 \\ -6.0 \end{pmatrix}$	$\begin{pmatrix} +3.1 \\ -2.4 \end{pmatrix}$ pb	27.6 ± 1.9 pb
$gg \rightarrow H$ (1-jet, $p_T^H < 60$ GeV)	4.4	$^{+4.8}_{-4.5}$	$\begin{pmatrix} +4.4 \\ -4.1 \end{pmatrix}$	$\begin{pmatrix} +1.7 \\ -1.8 \end{pmatrix}$ pb	6.6 ± 0.9 pb
$gg \rightarrow H$ (1-jet, $60 \leq p_T^H < 120$ GeV)	4.6	$^{+2.8}_{-2.4}$	$\begin{pmatrix} +2.7 \\ -2.4 \end{pmatrix}$	$\begin{pmatrix} +0.7 \\ -0.5 \end{pmatrix}$ pb	4.6 ± 0.7 pb
$gg \rightarrow H$ (1-jet, $120 \leq p_T^H < 200$ GeV)	1.6	$^{+1.1}_{-0.9}$	$\begin{pmatrix} +1.0 \\ -0.9 \end{pmatrix}$	$\begin{pmatrix} +0.3 \\ -0.2 \end{pmatrix}$ pb	0.75 ± 0.15 pb
$gg \rightarrow H$ (≥ 2 -jet, $p_T^H < 200$ GeV or VBF-like)	10.6	$^{+4.7}_{-4.2}$	$\begin{pmatrix} +4.3 \\ -3.9 \end{pmatrix}$	$\begin{pmatrix} +1.9 \\ -1.4 \end{pmatrix}$ pb	4.8 ± 1.0 pb
$gg \rightarrow H$ (≥ 1 -jet, $p_T^H \geq 200$ GeV) + $qq \rightarrow Hqq$ ($p_T^j \geq 200$ GeV)	1.9	$^{+0.9}_{-0.7}$	$\begin{pmatrix} +0.8 \\ -0.7 \end{pmatrix}$	$\begin{pmatrix} +0.3 \\ -0.2 \end{pmatrix}$ pb	0.81 ± 0.16 pb
$qq \rightarrow Hqq$ ($p_T^j < 200$ GeV)	9.8	$^{+4.3}_{-3.5}$	$\begin{pmatrix} +4.0 \\ -3.2 \end{pmatrix}$	$\begin{pmatrix} +1.5 \\ -1.4 \end{pmatrix}$ pb	$4.58^{+0.15}_{-0.18}$ pb
$gg/qq \rightarrow H\ell\ell/H\ell\nu$	0.2	$^{+0.9}_{-0.7}$	$\begin{pmatrix} +0.8 \\ -0.7 \end{pmatrix}$	± 0.2 pb	$0.63^{+0.03}_{-0.06}$ pb
$q\bar{q}/gg \rightarrow t\bar{t}H$	0.3	$^{+0.5}_{-0.4}$	$\begin{pmatrix} +0.5 \\ -0.4 \end{pmatrix}$	± 0.1 pb	$0.59^{+0.04}_{-0.05}$ pb

Table 2: Best-fit values and uncertainties of the ratio of branching ratios $B_{H \rightarrow \gamma\gamma}/B_{H \rightarrow 4\ell}$ and of the simplified template cross sections. The SM predictions are shown for each region.

3.6 κ framework

The κ framework expresses the product of cross sections and branching ratios ($\sigma \times B$) in terms of coupling modifiers κ [10]:

$$\sigma_i \times B(H \rightarrow f) = \frac{\kappa_i^2 \kappa_f^2}{\kappa_H^2} \sigma_i^{SM} \times B^{SM}(H \rightarrow f) \quad (3.2)$$

where i and f are the initial and final states, respectively, σ_i^{SM} is the SM production cross section, and $B^{SM}(H \rightarrow f)$ is the SM value of the branching ratio ($H \rightarrow f$). In the absence of non-SM decays the coefficient to the Higgs boson width, κ_H , is a function of the other κ parameters; similarly, in the absence of non-SM loops in the effective Hgg and $H\gamma\gamma$ couplings, the corresponding coefficients κ_g and κ_γ are functions of the other parameters. Three models are tested using progressively relaxed assumptions on the coupling relationships.

In the first model, a two-parameter fit of κ_f and κ_V is performed. The $H \rightarrow ZZ^* \rightarrow 4\ell$ branching fraction is proportional to κ_V^2 , while the $H \rightarrow \gamma\gamma$ branching fraction depends on κ_f^2 , κ_V^2 , and $\kappa_V \kappa_f$ due to significant contributions from top-quark and W-boson loops, and their interference, in the decay. Both branching fractions are inversely dependent on these three κ combinations through the total width of the Higgs boson. The dominant production mechanisms of ggF and VBF depend on κ_f^2 and κ_V^2 , respectively. The branching fraction to new states is assumed to be zero. The fit results are summarised in Figure 3 (left) and show a positive correlation of 54% due in part to the destructive interference between the top-quark and W-boson loops in the $H\gamma\gamma$ decay. The best-fit values and uncertainties are $\kappa_V = 1.03 \pm 0.06$ and $\kappa_f = 0.89_{-0.15}^{+0.20}$. The two-dimensional compatibility with the SM prediction is $p_{SM} = 52\%$.

In the second model, the effective couplings κ_g and κ_γ capture all loop contributions to the Higgs-boson interaction with gluons and photons, respectively. New loop processes would appear in these modifiers rather than being absorbed by the κ_f and κ_V modifiers. In this model, production and decay modes other than ggF, $H \rightarrow gg$ and $H \rightarrow \gamma\gamma$ are fixed to their SM expectations. Similar to the first model, the branching fraction to new states is assumed to be zero. The two-parameter fit for κ_g and κ_γ shows a strong anti-correlation of -64% because the leading constraint comes from $H \rightarrow \gamma\gamma$ in the gluon fusion channel. The best-fit values and uncertainties are $\kappa_g = 1.08_{-0.10}^{+0.11}$ and $\kappa_\gamma = 0.93_{-0.08}^{+0.09}$. The two-dimensional compatibility with the SM prediction is $p_{SM} = 68\%$.

Finally, a generic model based on a set of four ratios is constructed to probe the loop vertices (κ_g , κ_γ), total width (κ_H), and the fermion and vector couplings (κ_f , κ_V): $\kappa_{gV} = \kappa_g \kappa_V / \kappa_H$, $\lambda_{Vg} = \kappa_V / \kappa_g$, $\lambda_{fg} = \kappa_f / \kappa_g$, and $\lambda_{\gamma V} = \kappa_\gamma / \kappa_V$. The inclusion of κ_H in the parameterisation allows for non-SM decays of the Higgs boson. The results are summarised in Figure 3 (right). The four-dimensional compatibility with the SM prediction is $p_{SM} = 15\%$.

4. Conclusions and Outlook

Measurements of Higgs boson production cross sections and branching ratios have been presented for the combination of $H \rightarrow \gamma\gamma$ and $H \rightarrow ZZ^* \rightarrow 4\ell$ decay channels based on 36.1 fb^{-1} of proton-proton collision data recorded during 2015 and 2016 at $\sqrt{s} = 13 \text{ TeV}$ by the ATLAS experiment at the LHC. No significant deviations from the Standard Model expectations are observed.

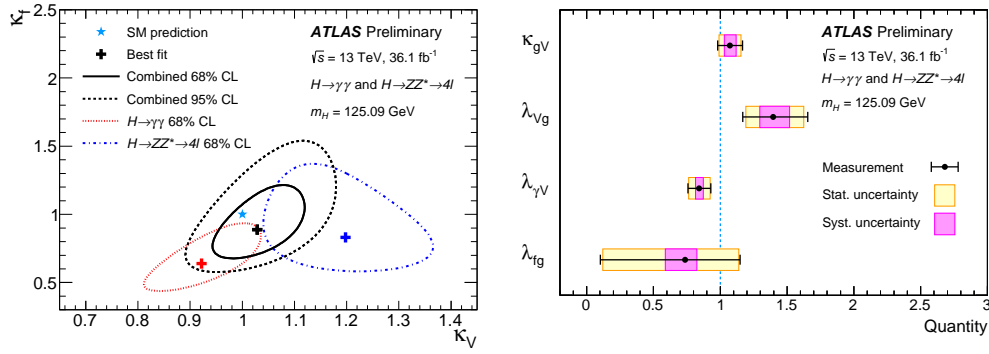


Figure 3: (Left) contours at 68% and 95% CL in the (κ_f, κ_V) plane for the individual decay modes $H \rightarrow ZZ^* \rightarrow 4\ell$ (blue) and $H \rightarrow \gamma\gamma$ (red), and the combination (black). The SM prediction is shown as a blue star and lies within the 68% contour of the best fit combined values [6]. (Right) best-fit values and uncertainties of κ_{gV} , λ_{Vg} , λ_{fg} , and $\lambda_{\gamma V}$. All parameters are defined to be unity in the SM [6].

Some tensions at the level of 2σ can be observed in the VBF production cross section compared to the SM prediction, but all compatibility p-values are a few percents or higher. The first measurements using a simplified version of “stage-1” STXS have been performed. The sensitivity to finer splitting of kinematics is expected to increase with higher data statistics.

References

- [1] ATLAS Collaboration, Phys. Lett. B 716 (2012) 1.
- [2] CMS Collaboration, Phys. Lett. B 716 (2012) 30.
- [3] ATLAS and CMS Collaborations, JHEP 1608 (2016) 045.
- [4] ATLAS Collaboration, <https://cds.cern.ch/record/2206272>, ATLAS-CONF-2016-081 (2016).
- [5] CMS Collaboration, <https://cds.cern.ch/record/2257530>, CMS-PAS-HIG-17-015 (2017).
- [6] ATLAS Collaboration, <https://cds.cern.ch/record/2273854>, ATLAS-CONF-2017-047 (2017).
- [7] ATLAS Collaboration, <https://cds.cern.ch/record/2273852>, ATLAS-CONF-2017-045 (2017).
- [8] ATLAS Collaboration, <https://cds.cern.ch/record/2265796>, ATLAS-CONF-2017-032 (2017).
- [9] D. de Florian et al., LHC Higgs Cross Section Working Group, arXiv: 1610.07922 [hep-ph] (2016).
- [10] S. Heinemeyer et al., LHC Higgs Cross Section Working Group, arXiv: 1307.1347 [hep-ph] (2013).